Stretching DNA by electric field and flow field in microfluidic devices: An experimental validation to the devices designed with computer simulations

Cheng-Han Lee and Chih-Chen Hsieh[a)]
Department of Chemical Engineering, National Taiwan University, Taipei, 106 Taiwan

(Received 15 December 2012; accepted 25 January 2013; published online 8 February 2013)

We examined the performance of three microfluidic devices for stretching DNA. The first device is a microchannel with a contraction, and the remaining two are the modifications to the first. The modified designs were made with the help of computer simulations [C. C. Hsieh and T. H. Lin, Biomicrofluidics **5**(4), 044106 (2011) and C. C. Hsieh, T. H. Lin, and C. D. Huang, Biomicrofluidics **6**, 044105 (2012)] and they were optimized for operating with electric field. In our experiments, we first used DC electric field to stretch DNA. However, the experimental results were not even in qualitative agreement with our simulations. More detailed investigation revealed that DNA molecules adopt a globular conformation in high DC field and therefore become more difficult to stretch. Owing to the similarity between flow field and electric field, we turned to use flow field to stretch DNA with the same devices. The evolution patterns of DNA conformation in flow field were found qualitatively the same as our prediction based on electric field. We analyzed the maximum values, the evolution and the distributions of DNA extension at different Deborah number in each device. We found that the shear and the hydrodynamic interaction have significant influence on the performance of the devices. © *2013 American Institute of Physics*.
[http://dx.doi.org/10.1063/1.4790821]

INTRODUCTION

DNA as the core hereditary material contains the genetic instructions for the development and functioning of all known living organisms and some viruses. The knowledge of the complete DNA sequence of a living organism is of invaluable importance. However, in many applications, only the existence and the locations of certain sequences are important. For example, comparative genomics[3] use this information to study the evolution of species and gene function. For forensic scientists, repetitive DNA sequences, particularly short tandem repeats (STRs), are used to determine the identity of individuals.[4]

An efficient and straightforward way to obtain the coarse DNA sequence information called "direct linear analysis (DLA)" was developed by Chen and coworkers.[5–7] The core idea of the DLA is to tag specific short sequences with fluorescent probes, and then to stretch DNA to locate these short sequences from the binding sites of the fluorescent tags. These tags on DNA act like a barcode system that allows one to recognize the identity of the DNA. To implement this DNA barcode system, finding an efficient and reliable method to stretch DNA is crucial. Although different approaches are available,[8–13] the most popular choice is to stretch DNA by either flow or electric field in a microfluidic device with a microcontraction.[5–7,14,15] Such a device can stretch DNA in a continuous process, and therefore it is capable of providing a very high throughput. Moreover, the device is of low cost and requires no special equipment to operate. However, the main problems to overcome in order to stretch DNA to a high degree using microcontraction are the shear component of the field[5] and molecular individualism.[16] The

[a)]Author to whom correspondence should be addressed. Electronic mail: ccjhsieh@ntu.edu.tw.

former, caused by the no-slip boundary conditions in a fluid flow, induces tumbling motion of DNA that prevents it from accumulating elongational deformation.[17] The latter, a presentation of the entropy effect to molecular conformation, leads to a broad distribution of DNA extension on the basis that the same amount of strain is provided.

Different ways to overcome these problems have been proposed in the literatures. To avoid shear, electric field is preferred over flow field because electric field induced electrophoretic velocity in an insulated device is purely elongational or shear-free.[18] As a result, DNA in electric field experiences pure elongational deformation. The molecular individualism, however, is more difficult to deal with. The major consequence of the molecular individualism is that each DNA requires different amount of strain to reach the plateau extension. A common approach to alleviate this problem is to "pre-condition" DNA so they adopt conformations more suitable for being stretched. Various conformation preconditioning strategies found in the literature include pre-shearing DNA,[19] passing DNA through a gel matrix[7] or obstacle arrays,[15,20] and exposing DNA to an oscillating extensional flow.[19] However, these methods are either troublesome to apply or having vary limited benefit. A more detailed discussion about the advantages and disadvantages of these preconditioning methods was given in our previous paper.[1]

In our previous studies,[1,2] we have employed the Brownian dynamics simulations and finite element method[1,2,21–23] to guide the design and the optimization of a microcontraction based DNA stretching microfluidic device. Our simulations were performed with the assumptions that DNA was driven electrophoretically through the device and any nonlinear electrokinetic phenomena[24,25] was neglected. Earlier simulations with the same assumptions yielded results in good agreement with the experimental data at small to moderate electric field (or Deborah number (De)).[20,23,26] With the help of computer simulations, we developed a new pre-conditioning approach called "pre-stretching."[1] The approach uses an expansion in front of the microcontraction to generate an electric field gradient to pre-stretch DNA. Our simulations predicted that DNA will be stretched in the direction perpendicular to the contraction funnel at the expansion, and they then will be turned by the electric field to align with the funnel direction for the successive stretching. As a result, DNA will be stretched two times and reach a higher extension. We have designed two microfluidic channels that were integrated with the "pre-stretch" approach. In this study, we aim to realize our designs and to examine our prediction against experiments. We also want to find hints for how to improve our simulation procedure from the difference between experiments and simulations.

The three DNA stretching devices to test are denoted as case I, case II, and case III. The schematic diagram of these devices is given in Fig. 1, and the design parameters are listed in Table I. Case I is simply a uniformly wide microchannel connected with a microcontraction (Fig. 1(a)), and it will serve as the base case for comparison. The exact shape of the contraction was taken from the study of Randall *et al.*,[7] and it was also used in the rest two cases. Case II and case III are the designs generated from our previous studies[1,2] with the help of computer simulations. Case II (Fig. 1(b)) has an expansion set before the contraction for pre-stretching DNA. Our simulations[1] predicted that this design can significantly improve DNA extension over case I. However, we later found also by simulations[2] that the efficiency of case II will deteriorate with increasing DNA molecular weight due to DNA folding when they flowing along the axial region of the device. Case III shown in Fig. 1(c) was designed to remedy this problem. The shape of case III is simply a half of case II, and its design principle is to prevent DNA from passing the axial region by simply removing that part of the domain. Case III was predicted[2] to outperform both case I and case II for stretching both small (λ-DNA) and large DNA (T4-DNA). We note that the main part responsible for stretching DNA in case II and case III is between $x/l_c = -1$ and 2.375, corresponding to the end of the contraction and the beginning of the expansion. Although we only considered the DNA behavior in the main part of the devices in the simulations, in reality, it is necessary to have an inlet channel connecting the reservoir to the expansion. From Figs. 1(b) and 1(c), the inlet channels consist of three parts from the reservoir: a wide part, a very long and slightly tapered channel, and a long but narrow channel connecting to the main part of the device. This design is to prevent DNA from being stretched before they enter the expansion.

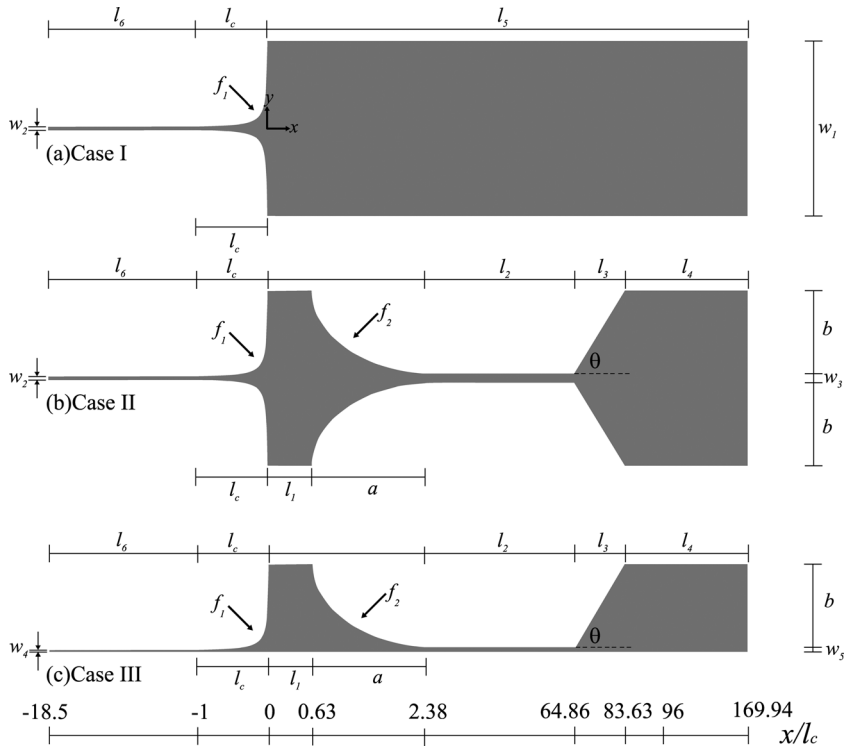

FIG. 1. The schematic diagram of the devices used in this study. (a) Case I: contraction only, (b) case II: contraction with an expansion for pre-stretching DNA, (c) case III: A modification of case II to prevent DNA from passing the region near the axis of case II. The height of all three devices is 2 μm in the z direction (not shown). All dimensions in the figure are in proportion except l_2, l_3, l_4, l_5, and l_6 since they are much longer than the rest. The tapered angle θ is about 3.6° so the field gradient is not strong enough to stretch DNA in the inlet conduit. The numerical values of the design parameters are listed in Table I. The scale bar at the bottom of the figure marks the dimensionless x-coordinate (x/l_c) at critical places for readers' reference.

As described above, our devices and experimental arrangement were specifically designed for operating with electric field. However, as will be revealed in the results section, the experimental results deviated significantly from our predictions. We have determined that the major cause of the deviation was a mysterious phenomenon that makes DNA to adopt a globular conformation in high DC electric field. Instead of giving up the project, we turned to use flow field to stretch DNA. We expect that case II and case III should still work better than case I even if the driving force becomes flow field. In other words, we expect that the extension-rotation motion which gives rise to the preconditioning effect should still exist in flow field because the variation of the major components of the flow field is qualitatively similar to those of electric field.

TABLE I. The design parameters of the three testing devices.

w_1	200 μm	w_5	5 μm	l_4	6905 μm	a	140 μm
w_2	3.8 μm	l_1	50 μm	l_5	8595 μm	b	95 μm
w_3	10 μm	l_2	5000 μm	l_6	1400 μm		
w_4	1.9 μm	l_3	1500 μm	l_c	80 μm		

$$f_1 = \frac{w_1}{2\left(\frac{-x}{l_c}\left(\frac{w_1}{w_2} - 1\right) + 1\right)}; \quad f_2 = 100 - b\sqrt{1 - \frac{(190 - x)^2}{a^2}}$$

EXPERIMENTS

We used soft lithography to construct the microfluidic channels. The channels were replicated from a mold by curing polydimethysiloxane (PDMS, Sylgard 184, Dow Corning) at 65 °C for 12 h. The molds were made on silicon wafers patterned with AZ5214E photoresist (Clariant) using standard photolithography techniques. The thickness of the photoresist is 2 μm and it defines the height of microfluidic channels. To prepare the flow cell, we cut a channel from the cured PDMS and built reservoirs at both ends of the channel. The PDMS channel was then bound to a clean glass coverslip by treating both with oxygen plasma for 30 s before bounding. This bounding was strong enough to hold the assembly without leak under the pressure used in our experiments (typically below 3 psi). The coverslip bounded PDMS channel was soaked in 2X TBE buffer for 12 h before the experiments. This step was to prevent the permeation-driven flow[27] from disturbing the flow field inside the channel. However, the permeation-driven flow will appear once the PDMS becomes dry. Therefore, we always finished an experiment within two hours so the permeation-driven flow had negligible effects to our results.[15]

T4GT7 DNA (165.6 kbp, Nippon Gene) used in this study was stained with YOYO-1 (Invitrogen) at the ratio of 4 base pair:1 dye molecule. The contour length L of the stained T4-DNA was 70 μm.[15] The experimental buffer was 2 × TBE with 30% sucrose (Sigma-Aldrich) and 4% β-mercaptoethanol (Sigma-Aldrich). For all experiments, the buffer solutions were viscosified with sucrose to increase DNA relaxation time. The viscosity of the viscosified buffer solutions was measured to be 4.7cp at 25C using both capillary viscometer and Brookfield DV-III ultra viscometer. For experiments with electric field, the buffer solutions contained additional 0.07% PVP (polyvinylpyrrolidone, Polysciences, MW = 10 000) for dynamically coating the microchannel surface to suppress the electroosmosis flow.[7,18] To stretch DNA with electric field, two platinum electrodes were placed in the reservoirs and a desired voltage was applied by a DC power supplier (Gwinstek GPS2303). To stretch DNA with flow field, a constant pressure was applied to the solutions in the inlet reservoir by nitrogen from a gas cylinder. The pressure was monitored by a digital gauge (Ashcroft, type 2030) to ensure the constant value through the experiments. The dynamics of DNA was observed using an Olympus IX-71 inverted microscopy through a 60× 1.35 NA oil-immersed objective. A 200 W metal-halide lamp (Prior, Lumen 200) attenuated to its 12.5% output was used as the light source. The fluorescence microscopy images were captured using Hamamatsu EMCCD (model: C9100-13) at 0.0313 s/frame. Our setup yielded a field-of-view of 136.5 μm × 136.5 μm. Since the field of view is smaller than the region of interest for most situations in our experiments, often several views had to be taken to provide the complete information of DNA evolution in the devices.

The major interest to measure in this study is the DNA extension L_{ex} as a function of its x-coordinate. Here, L_{ex} is defined as the distance between the maximum coordinates (x_{max}, y_{max}) and the minimum coordinates (x_{min}, y_{min}) of the DNA molecule, and the x-coordinate of a DNA is defined by its x_{max}. We emphasize that L_{ex} defined here is not the exact DNA extension measured along its contour but is an approximation to the true extension for easier measurement. Since the same definition for L_{ex} and for the x-coordinate of a DNA has been used in the previous experiments[7,15] and simulations,[1,2,23] a cross comparison between the current and the past studies can be made on the same basis. To compare our results with the related studies, the strain rate has also to be converted to the dimensionless strain rate, or Deborah number. Following the previous studies,[1,2,7,23] the characteristic De is defined to be the nominal De in the contraction. Formally, the characteristic De should be calculated by $De = \tau\dot{\varepsilon} = \tau(\frac{v_{outlet} - v_{inlet}}{l_c})$. Here, v_{inlet} and v_{outlet} are the flow velocity (or the electrophoretic velocity in electric field) at the inlet ($x/l_c = 0$) and the outlet ($x/l_c = -1$) of the contraction, respectively. τ is the longest relaxation time of DNA and l_c is the length of the contraction. Since v_{inlet} is much smaller than v_{outlet}, we further neglect v_{inlet} and calculate De as $De = \tau(\frac{v_{outlet}}{l_c})$. The same approximation has also been made in the previous studies.[1,2,7,23] In this study, the v_{outlet} was determined experimentally by measuring DNA velocity in the device. However, since DNA moved very fast in the contraction, we instead measured the velocity of DNA at the wide part of the inlet channel ($v_{widepart}$) to infer v_{outlet}. Since the fluid is incompressible, $v_{outlet}/v_{widepart}$ should be equal to the

ratio between the widths of the two parts. In our experiments, $v_{widepart}$ was typically measured at $x/l_c \approx 96$ (Fig. 1), and the applied voltage or pressure was tuned until the desired *De* was achieved.

To calculate the Deborah number, we also had to determine the longest relaxation time τ of T4- DNA in our experimental condition. To do so, T4-DNA was stretched by electric field in a 2 μm high, 40 μm wide cross-slot channel similar to that used in Juang *et al.*[28] Once a DNA was stretched over 50% of the contour length, the electric field was turned off and the change of DNA conformation was recorded as a function of time. We obtained the DNA relaxation time by fitting the time evolution of the ensemble averaged DNA extension to a single exponential function:[22]

$$\frac{\langle x_{ex}(t)^2\rangle - \langle x_{ex}(t)^2\rangle_0}{L^2} = A\exp(-t/\tau), \tag{1}$$

where $x_{ex}(t)$ is the projection of the DNA length in the stretching direction, $\langle\ \rangle$ represents an ensemble average of multiple chains, $\langle x_{ex}(t)^2\rangle_0$ is the equilibrium value of $x_{ex}(t)^2$, and A is a fitting parameter. When $x_{ex}(t)$ becomes smaller than 30% of the contour length, we fit Eq. (1) to obtain τ. Fig. 2 shows the squared relative extension of 15 T4-DNA molecules (thin lines) and their ensemble average (thick line). The fitting line is expressed by the dashed line and the T4-DNA relaxation time in the 1 cp buffer was τ= 1.33 s. The experimental value of $\langle x_{ex}(t)^2\rangle_0$ was measured to be 21 μm^2 in our 2 μm-high microfluidic channel, consistent with the value reported by Randall *et al.*[7] under the same experimental condition.

RESULTS AND DISCUSSIONS

Stretching DNA with electric field

As the startup of this study, we first performed DNA stretching experiments using electric field at *De* = 7, 14 and 23 for case II. The ensemble averaged maximum DNA extension versus *De* was plotted in Fig. 3. Also given in Fig. 3 are the experimental results for case I from Randall *et al.*[7] and our simulation predictions[2] for case I and case II. As can be seen in Fig. 3, our experimental results were much lower than the simulation predictions. Moreover, the experimentally measured DNA extension in case II is also consistently lower than that in case I at all available *De*. Even more strangely, the DNA extension in case II reaches a maximum at *De* = 14 and starts to decrease with *De*. This was entirely out of our expectation and seemed to violate the common scenario that the maximum DNA extension increases with *De*. However, our qualitative experiments in cases III showed the same trend. Therefore, we were convinced

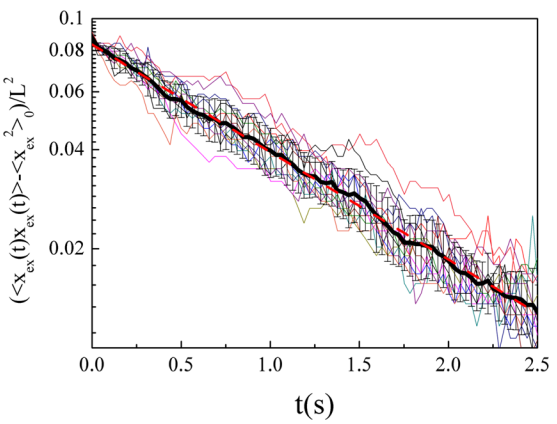

FIG. 2. The relaxation of T4-DNA in 1 cp buffer solution. Each thin line represents a single DNA relaxation curve. The thick line is the ensemble average of 15 T4-DNA relaxation curves, and the dashed line is the single exponential fitting to the average. The relaxation time of T4-DNA is found to be 1.33 s.

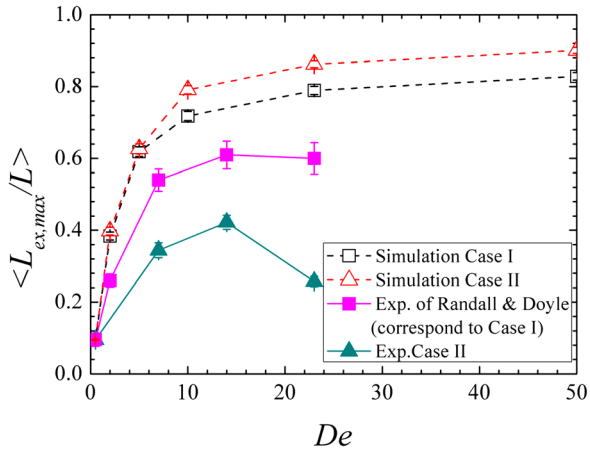

FIG. 3. The simulated (hollow symbols) and experimental (filled symbols) maximum ensemble averaged relative T4-DNA extension obtained in the case I and case II at $De = 0$, 7, 14, and 23 in electric field. The experimental results for case I are taken from Randall *et al.*[7]

that some phenomenon beyond the common assumptions for this situation was happening in our experiments.

To determine the cause of this unexpected result, we examined DNA images taken at $De = 23$ in case II (see Fig. 4). Based on our simulations, we expected that DNA at the expansion should be partially stretched, but DNA in Fig. 4 actually adopted a globular, rather compact conformation. Moreover, DNA maintained the same conformation through the whole expansion region and only extended very little even when entering the contraction. To trace the origin of this phenomenon, we examined DNA conformation in the inlet channel and found that DNA only adopt the globular conformation after moving into the narrow part of the inlet channel ($x/l_c = 2.38 \sim 64.86$). Since the electric field in the narrow part of the inlet channel is uniform, the phenomenon was not caused by the electric field gradient. However, we noticed that this phenomenon was absent at very low *De* (or electric field) and it only becomes evident when the electric field in the channel was over a threshold about 100 V/cm. We searched the literature and found that the same phenomenon has just been reported very recently by Tang *et al.*[29] They found that DNA coil was compressed into an isotropic globule in a uniform but relatively high DC electric field. They also showed that the shrinkage of DNA coil in 2.5X TBE buffer starts at the electric field as low as 50 V/cm. More importantly, they reported that DNA, once compressed into globule, become much more difficult to stretch. We estimated that the electric field in the narrow part of the inlet channel of case II was about 123, 246, and 404 V/cm at $De = 7$, 14, and 23, respectively. Thus, our observation is quantitatively consistent with that reported by Tang *et al.*[29] However, the cause of this phenomenon is still not understood. Since case I does not have the narrow inlet channel, DNA coil maintains the equilibrium conformation before going into the contraction. This also explains why the DNA extension measured in case II is consistently lower than those measured in case I.

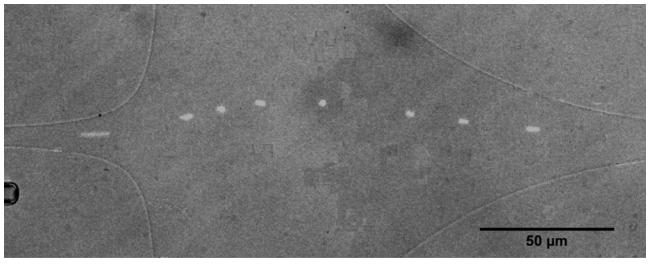

FIG. 4. A time-lapse image of a typical T4-DNA passing case II in the electric field at $De = 23$.

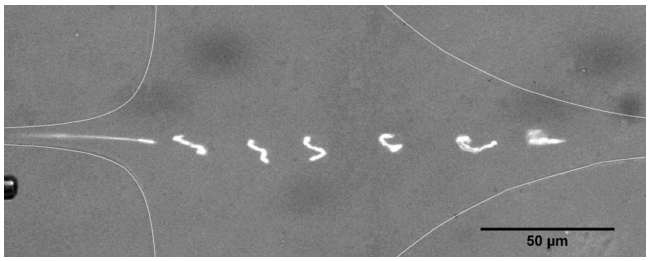

FIG. 5. A time-lapse image of a typical T4-DNA passing case II in the flow field at $De = 20$.

Stretching DNA with flow field

As mentioned in the Introduction, after the failure to stretch DNA using electric field with our newly designed devices, we turned to use flow field to stretch DNA. In order to make sure the flow field could do the job and to gain some physical insights, we first examined qualitatively the DNA dynamics in case II and case III. Fig. 5 is the time-lapse image of a T4-DNA in case II at $De = 20$ in flow field. As can be seen, the DNA molecule was partially stretched in x direction when it left the inlet channel and entered the expansion. DNA is partially stretched due to the strong shear in the inlet channel. At the expansion, the flow slowed down in x direction and accelerated in the y direction. Therefore, DNA was compressed in x direction and stretched in y direction. Since DNA was already stretched in x direction, its extension first decreased and then rebounded as the process proceeded. At the end of the expansion, DNA has become partially stretched in y direction. Between the expansion and the contraction, DNA experienced a rotational motion that made the DNA segments closest to the center axis enter the contraction earlier than the rest segments. As DNA entered the contraction, it becomes highly stretched. This result ensured us that the flow field is capable of stretching DNA.

In our experiments with flow field in case II, we also observed two distinct evolution patterns of DNA conformation that have been predicted by our simulations.[1,2] The representative images of these two types of conformation evolution are shown in Fig. 6. In Fig. 6(a), the DNA molecule was stretched at the expansion and then underwent a rotational motion between the expansion and the inlet of the contraction. This rotational motion allows DNA to preserve the extension originally achieved in y direction to x direction, and therefore it is the key to the preconditioning effect. This rotational motion only happened when DNA passing off the center

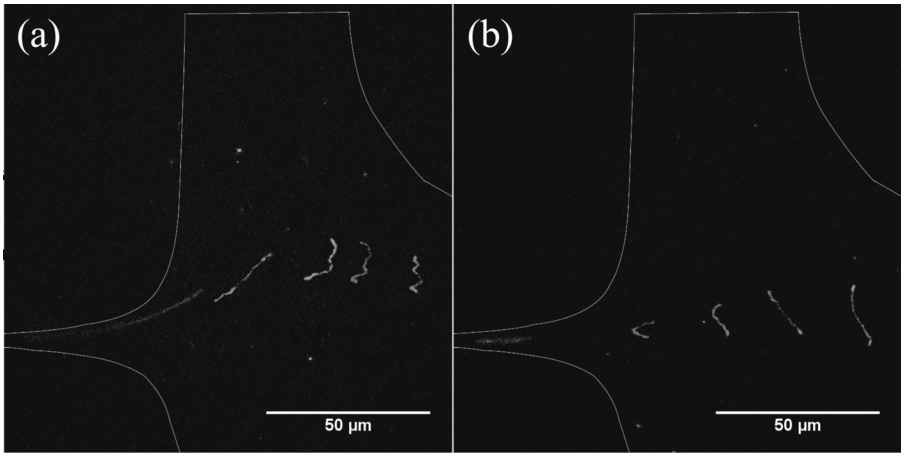

FIG. 6. Two representative evolution patterns of T4-DNA in the case II in the flow field. (a) A DNA undergoes the extension-rotation motion, (b) a DNA was stretched at the expansion but adopted a folded conformation at the inlet of the contraction. The images were taken at $De = 20$. The edges of the devices are very unclear in the original images so we drew the edge line for the reader's reference.

axis of the device, and these DNA can be stretched to a very high degree in the contraction. On the other hand, DNA molecules moving along the axial region, although pre-stretched at the expansion, were prone to fold (see Fig. 6(b)) at the entrance of the contraction. This is because DNA passing this region often has its segments on both sides of the axis. Since the DNA segments closer to the axis move faster than those farther from the axis, this velocity difference results in the formation of folded conformation and hinders the unraveling of DNA.[30] While the driving force in our previous simulations is different from that in current experiments, readers can still compare Fig. 6 with Figs. 4(d) and 4(e) of our previous study[2] to see how similarly the DNA behaves.

Case III was designed to avoid DNA folding in case II by preventing the segments of a DNA molecule from presenting on both sides of the axis. This strategy was proved working very effectively in the simulations based on electric field and was also found to work in flow field in our experiments. Consequently, the majority of DNA population was found having the evolution pattern the same as that shown in Fig. 6(a). However, we noticed that DNA in case III rarely passed the region near the side wall along $y = 0$ in the expansion region. This is qualitatively different from the simulation prediction that DNA population density gradually decreases with the distance from the bottom wall. We speculate that the depletion of DNA near the wall is the manifestation of the "shear-induced migration" phenomenon.[31,32] It is well known that DNA (or long chain polymer) molecules in strong pressure driven flow will migrate away from the solid boundary and form a depletion layer[33,34] due to the hydrodynamic interaction between extended DNA and the boundary.[31,35,36] The thickness of the depletion layer in bulk condition was shown to grow with the shear rate[31,33,37] and can be much larger than the radius of gyration of DNA. In our experiments, since the height of the device is smaller than the equilibrium size of T4-DNA in bulk solutions, the depletion layer will only be noteworthy on the side walls, but its thickness will be much reduced comparing to that in bulk because the confinement will weaken the hydrodynamic interactions.[38–40] We speculate that a thin depletion layer has been formed on the side walls in the inlet channel. Since the width of the channel increases from 5 μm in the inlet channel to 100 μm at the expansion, the spreading of streamlines results in a much more significant depletion area at the expansion.

Another phenomenon that was only observed in flow field but has never been seen in electric field or in our simulations is a "flip" motion of DNA in the contraction channel. The flip motion means that a stretched DNA switches its head with its tail in the flow field. The "normal" and the "flip" motion of DNA were displayed in Figs. 7(a) and 7(b), respectively. This phenomenon happened when the front part of DNA was in touch with the curved side wall of the contraction. Due to the very low velocity near the boundary, the back part of DNA that stays farther from the boundary moves faster than the front part that is closer to the boundary. Consequently, the back part of DNA moves ahead of the front part and results in a "flip" motion. However, since the no-slip boundary condition also appears on the top and the bottom walls of the device, why does the flip motion only happen on the curved side wall? We believe the flip motion is actually a consequence of the well-known phenomenon of polymer migration in curvilinear flow,[41] first predicted and also observed by Dill and Zimm[42] using DNA in 1979. When a DNA molecule is stretched along a curvilinear streamline, it will migrate toward the center of the curvature. DNA migrates because the sum of the elastic force along its contour has a net component toward the center of the curvature of the contour. Applying above scenario to our devices, the flip motion will not occur on the top and bottom walls because they are flat. However, for DNA passing and stretching near the curved wall in the contraction, they will be pushed toward the wall and hence results in the flip motion. On the other hand, although DNA migration should also happen in electric field, there will be no flip motion of DNA due to the lack of no-slip boundary condition on the walls. When the flip motion was occurring, the extension of DNA declined since the distance between the front and the back parts of DNA must decrease during the flip. A characteristic signature of a flip motion can be found in the evolution of DNA extension shown by the medium thick lines in Fig. 7(c). As can be seen, the DNA extension suddenly dropped down and then went up again after some distance. We found that the flip motion was mostly happened in case I and rarely seen in other cases. The reason for

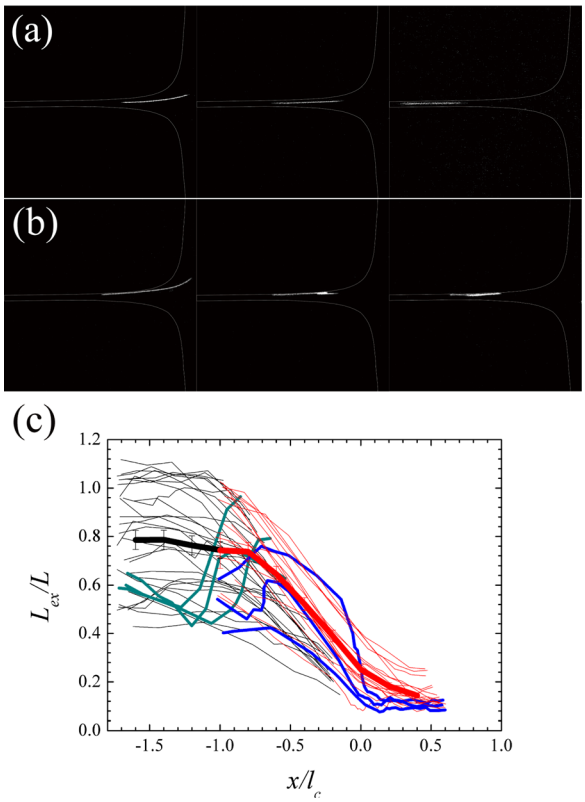

FIG. 7. The flip motion of DNA observed in case I in flow field. (a) Snapshots of DNA passing smoothly through the contraction, (b) snapshots of DNA undergoing a flip motion in the contraction, (c) the evolution of the extension of individual T4-DNA in case I in flow field at $De = 30$. The thin lines are the extension trajectories of DNA molecules that passed the contraction smoothly. The medium thick lines are the extension trajectories of DNA molecules that underwent the "flip" motion. The thickest line is the averaged extension of all DNA in this ensemble.

this seemingly bias is because the upstream shape of case II and case III excluded DNA from moving too close to the side walls in the contraction. We also found that the flip motion was seldom seen for De < 20, but happened more often for De $\geqq 20$. The thickest line in Fig. 7(c) is the averaged extension of T4-DNA. The unsmooth shape of the curve is caused by the DNA undergone the flip motion in its ensemble.

Having the qualitative picture in mind, we present the quantitative results in the following sections. Fig. 8 shows the evolution of DNA extension in all three devices and at different Deborah number. Each thin line in the figure represents the evolution of the extension of a single DNA. The ensemble averaged DNA extension was given by the thick lines. Since a field of view in our experimental setup was smaller than the region of interest, we had to take images from different areas to obtain the desired information. The results obtained from different fields of view were displayed in different colors. As can be seen in Fig. 8, although the curves of single DNA extension are discontinuous at the junctions between two fields of view, the curves of the ensemble averaged DNA extension connect very well. This indicates the consistency of our measurement. Since the major function of the device is to stretch DNA to its contour length, we focused on the contraction region where DNA shall reach their maximum extension. We only measured the DNA extension through the whole device in two representative cases for investigating the preconditioning effect of the devices, and the discussions will be presented later. Comparing the scattering of DNA extension trajectories with their means, we concluded that the "molecular individualism" of DNA was much reduced in case II and in case III than in case I. Actually, case III performs even better than case II in this aspect. This is also consistent with our expectation from the results of computer simulations.

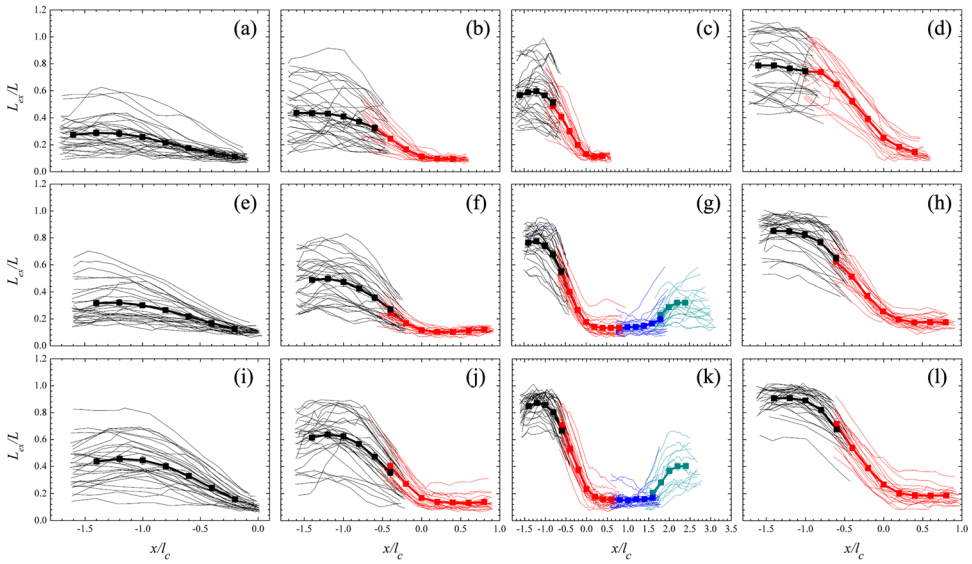

FIG. 8. The evolution of the DNA extension in case I ((a)–(d)), case II ((e)–(h)) and case III ((i)–(l)) at De = 5 ((a), (e), (i)), De = 10 ((b),(f), (j)), De = 20 ((c),(g),(k)) and De = 30 ((d),(h),(l)). Each thin line represents a single DNA extension trajectory and the thick lines represent the ensemble averaged DNA extension. Several different colors were used in some plots to represent the data measured from images taken from different fields of view.

In Fig. 9, we compare the evolution of the ensemble averaged DNA extension in each device at different *De*. It was found that DNA extension always increased monotonically with *De*. This observation was consistent with the theoretical prediction that higher Deborah number leads to a higher degree of DNA extension. From Figs. 9(b) and 9(c), DNA extension was found to approach a plateau value as *De* increased from 20 to 30. However, this was not observed in Fig. 9(a) because DNA in case I did not enjoyed the preconditioning effect and thus their averaged maximum extension was still far from the plateau value.

Figs. 10(a)–10(c) are the rearrangement of data in Fig. 9 to make a direct comparison of the evolution of the averaged DNA extension in each device. Also given in Figs. 10(d)–10(i) are the probability distribution of DNA extension at the inlet ($x/l_c = 0$) and the outlet ($x/l_c = -1$) of contraction. From Figs. 10(a)–10(c), we found that case III always performs the best, case II the second, and case I the third. This result again qualitatively agrees with the simulations with electric field. However, case II at $De = 10$ (Fig. 10(a)) performs only slightly better than case I. The probability distribution of DNA extension at the outlet (Fig. 10(g)) also confirms this fact. This is because the velocity gradient at the expansion is still low so the preconditioning effect is rather weak at this *De*. The probability distribution of DNA extension at the inlet of contraction (Fig. 10(d)) supports this scenario as well. When *De* increases to 20 (Fig. 10(b)), the preconditioning effect of case II is stronger (Fig. 10(e)) and the performance difference between case II and case I becomes more significant. As *De* increases to 30 (Fig. 10(c)), DNA extension is approaching the infinite strain limit, and the differences between the three cases become smaller. The data in Fig. 10(f) show that DNA in cases I and case II have very similar extension at the inlet of the contraction, indicating that DNA in case I was stretched in the inlet channel by the shear flow. Although at this *De* the DNA extension distributions in case I and in case II are very similar at the inlet of the contraction, they are very different at the outlet of the contraction due to the flip motion mentioned previously. Comparing to the simulation predictions, the performance differences between case I, case II, and case III are also smaller at $De = 30$. We believe that this is because the shear component of the flow field in the inlet channel provides some preconditioning effect to case I. On the other hand, the shear component in the inlet channel actually offset the preconditioning effect of case II and case III. Both effects help to reduce the performance differences between the three devices as *De* increases.

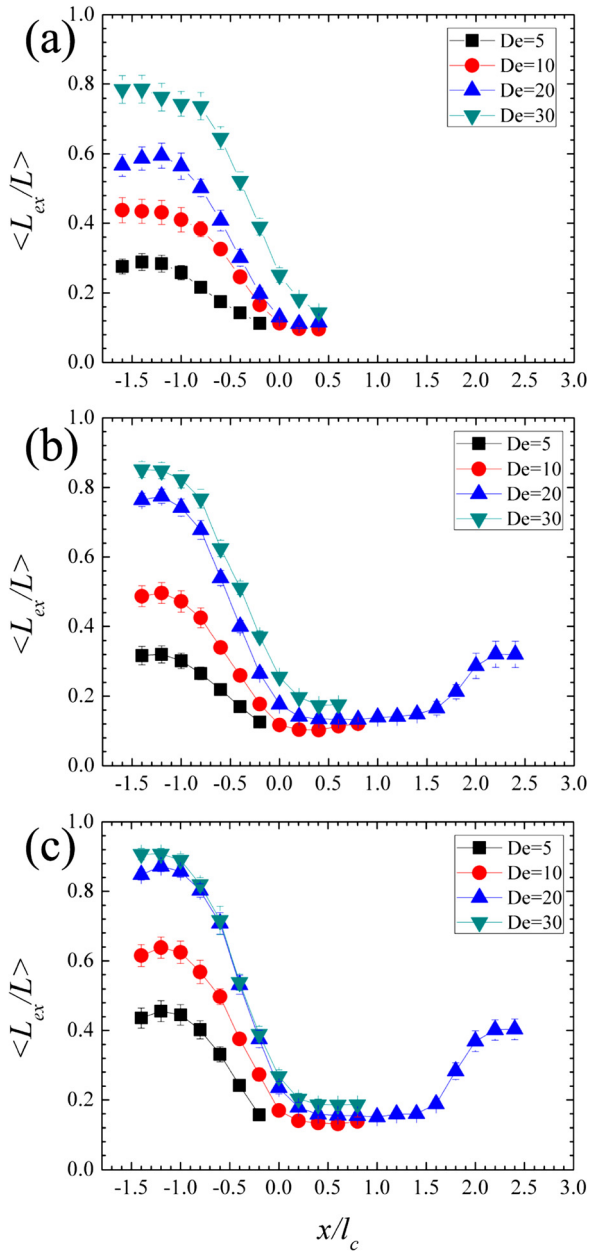

FIG. 9. The evolution of the ensemble averaged DNA extension in (a) case I, (b) case II, and (c) case III at different *De*.

To investigate the evolution of DNA extension in case II and case III, especially in the expansion region, we choose $De = 20$ as the representative cases and measured the DNA extension from the end of the inlet channel. As can be seen in Fig. 10(b), the relative DNA extension in the inlet channel is much higher than the equilibrium value due to the strong shear component there. DNA in case III extends more than in case II also due to the higher shear rate in case III. The DNA extension in both cases then starts to fall at the inlet of the expansion where $x/l_c \sim 2$. The falling of the DNA extension is because the flow gradient there was in y-direction, while DNA was extended in x-direction. DNA extension in both cases then reaches a nearly constant value in the range from $x/l_c = 1.3$ to 0.3 where the rotational motion of DNA is proceeding. For $x/l_c < 0.3$, the average DNA extension started to rise due to the flow gradient propagating from the contraction.

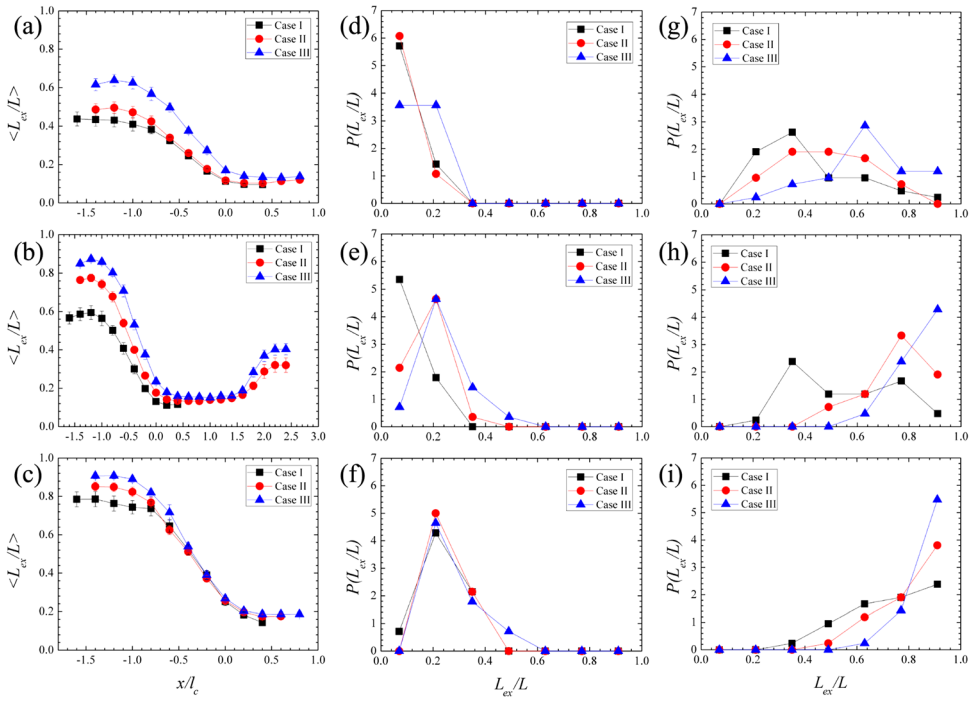

FIG. 10. The ensemble averaged relative T4-DNA extension at (a) $De = 10$, (b) $De = 20$, (c) $De = 30$ in three devices. The probability distributions of the relative DNA extension are also measured at the inlet ((d), (e), and (f)) and the outlet ((g), (h), and (i)) of the contraction for case I ((d), (g)), case II ((e), (h)), and case III ((f),(i)).

Finally, we summarize the maximum relative DNA extension at different *De* in three devices in Fig. 11. The results of homogeneous field represent the theoretical limit of DNA extension at the corresponding *De* with infinite strain.[15] For a more complete comparison, the maximum DNA extension in case I under electric field from the study of Randall *et al.*[7] was also plotted in Fig. 11. As can be seen, the performance of all devices in this study improves with increasing *De*. The performance of case III is already very close to the theoretical limit for $De \geq 20$. On the other hand, case I performs better with electric field than with flow field at low *De*. We believe that this is due to the shearless nature of electric field. However, the performance of case I with electric field levels off for $De > 10$ and eventually outpaced by case II

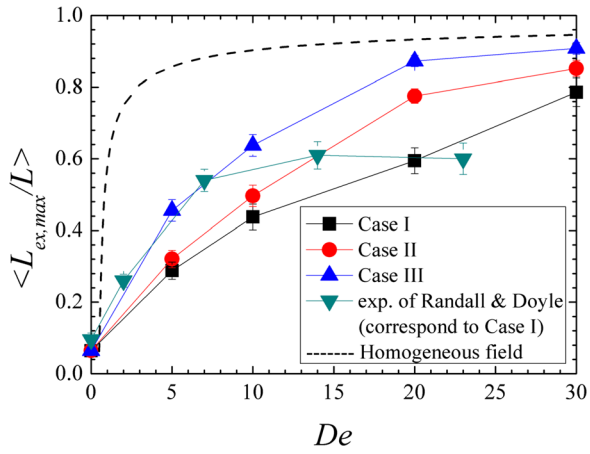

FIG. 11. The maximum ensemble averaged relative T4-DNA extension as a function of *De*. The dashed line represents DNA extension estimated under a constant field gradient (infinite strain limit). The experimental results of case I, case II, and case III are for flow field, and the results of Randall *et al.*[7] are for electric field.

and case III with flow field. We believe that the ceiling for the electrophoretic stretching of DNA is caused by the same phenomenon that causes DNA conformation change at high DC field.

CONCLUSIONS

We have experimentally examined the performance of two modified DNA stretching devices against their prototype device. The modified devices were designed specifically for operating with electric field and both were predicted to perform superior than the prototype device. However, we found experimentally that neither device has worked as expected. DNA molecules were actually more difficult to stretch in the modified devices because they adopted a globular conformation under high DC electric field encountered in the inlet channel. Instead of giving up the project, we tested the same devices for stretching DNA using flow field since the field kinematics is similar in electric field and flow field. However, evident differences also exist between two fields. The electric field is shearless, but the flow field has strong shear component. Moreover, the hydrodynamic interaction that has negligible influence on DNA behavior in electric field becomes more important in flow field. Nevertheless, DNA behavior in flow field was found very similar to our prediction based on electric field. The modified devices still preserve the "pre-stretch" preconditioning mechanism even when the driving force becomes flow field. Therefore, the main predictions from our computer simulations are still valid.

While our simulations with electric field did not yield correct predictions, its contribution should not be neglected. Without the simulation, it will be much more difficult for us to recognize the unexpected DNA conformation change. Finally, the most important lesson we learned from this study is that DNA behavior in electric field is far more complicate than we understood. It is necessary to further investigate the electric field influence on DNA and polyelectrolytes. The knowledge will be very important for the future design of biomicrofluidic devices.

ACKNOWLEDGMENTS

The authors thank the National Science Council of Taiwan for supporting this research under the grant of NSC 100-2628-E-002-029-MY2.

[1]C. C. Hsieh and T. H. Lin, Biomicrofluidics **5**(4), 044106 (2011).
[2]C. C. Hsieh, T. H. Lin, and C. D. Huang, Biomicrofluidics **6**, 044105 (2012).
[3]G. M. Rubin, M. D. Yandell, J. R. Wortman, G. L. G. Miklos, C. R. Nelson, I. K. Hariharan, M. E. Fortini, P. W. Li, R. Apweiler, W. Fleischmann, J. M. Cherry, S. Henikoff, M. P. Skupski, S. Misra, M. Ashburner, E. Birney, M. S. Boguski, T. Brody, P. Brokstein, S. E. Celniker, S. A. Chervitz, D. Coates, A. Cravchik, A. Gabrielian, R. F. Galle, W. M. Gelbart, R. A. George, L. S. B. Goldstein, F. C. Gong, P. Guan, N. L. Harris, B. A. Hay, R. A. Hoskins, J. Y. Li, Z. Y. Li, R. O. Hynes, S. J. M. Jones, P. M. Kuehl, B. Lemaitre, J. T. Littleton, D. K. Morrison, C. Mungall, P. H. O'Farrell, O. K. Pickeral, C. Shue, L. B. Vosshall, J. Zhang, Q. Zhao, X. Q. H. Zheng, F. Zhong, W. Y. Zhong, R. Gibbs, J. C. Venter, M. D. Adams, and S. Lewis, Science **287**(5461), 2204–2215 (2000).
[4]J. M. Butler, J. Forensic Sci. **51**(2), 253–265 (2006).
[5]E. Y. Chan, N. M. Goncalves, R. A. Haeusler, A. J. Hatch, J. W. Larson, A. M. Maletta, G. R. Yantz, E. D. Carstea, M. Fuchs, G. G. Wong, S. R. Gullans, and R. Gilmanshin, Genome Res. **14**(6), 1137–1146 (2004).
[6]K. M. Phillips, J. W. Larson, G. R. Yantz, C. M. D'Antoni, M. V. Gallo, K. A. Gillis, N. M. Goncalves, L. A. Neely, S. R. Gullans, and R. Gilmanshin, Nucleic Acids Res. **33**(18), 5829–5837 (2005).
[7]G. C. Randall, K. M. Schultz, and P. S. Doyle, Lab Chip **6**(4), 516–525 (2006).
[8]X. Michalet, R. Ekong, F. Fougerousse, S. Rousseaux, C. Schurra, N. Hornigold, M. vanSlegtenhorst, J. Wolfe, S. Povey, J. S. Beckmann, and A. Bensimon, Science **277**(5331), 1518–1523 (1997).
[9]A. Bensimon, A. Simon, A. Chiffaudel, V. Croquette, F. Heslot, and D. Bensimon, Science **265**(5181), 2096–2098 (1994).
[10]W. Reisner, K. J. Morton, R. Riehn, Y. M. Wang, Z. N. Yu, M. Rosen, J. C. Sturm, S. Y. Chou, E. Frey, and R. H. Austin, Phys. Rev. Lett. **94**(19), 196101 (2005).
[11]J. O. Tegenfeldt, C. Prinz, H. Cao, S. Chou, W. W. Reisner, R. Riehn, Y. M. Wang, E. C. Cox, J. C. Sturm, P. Silberzan, and R. H. Austin, Proc. Natl. Acad. Sci. U. S. A. **101**(30), 10979–10983 (2004).
[12]S. F. Lim, A. Karpusenko, J. J. Sakon, J. A. Hook, T. A. Lamar, and R. Riehn, Biomicrofluidics **5**(3), 034106 (2011).
[13]S. W. Hu, Y. J. Sheng, and H. K. Tsao, Biomicrofluidics **6**(2), 024130 (2012).
[14]J. W. Larson, G. R. Yantz, Q. Zhong, R. Charnas, C. M. D'Antoni, M. V. Gallo, K. A. Gillis, L. A. Neely, K. M. Phillips, G. G. Wong, S. R. Gullans, and R. Gilmanshin, Lab Chip **6**(9), 1187–1199 (2006).
[15]A. Balducci and P. S. Doyle, Macromolecules **41**(14), 5485–5492 (2008).
[16]P. G. deGennes, Science **276**(5321), 1999–2000 (1997).
[17]D. E. Smith, H. P. Babcock, and S. Chu, Science **283**(5408), 1724–1727 (1999).

[18]G. C. Randall and P. S. Doyle, Phys. Rev. Lett. **93**(5), 058102 (2004).
[19]R. G. Larson, J. Non-Newtonian Fluid Mech. **94**(1), 37–45 (2000).
[20]D. W. Trahan and P. S. Doyle, Biomicrofluidics **3**(1), 12803 (2009).
[21]C. C. Hsieh, S. J. Park, and R. G. Larson, Macromolecules **38**(4), 1456–1468 (2005).
[22]J. M. Kim and P. S. Doyle, J. Chem. Phys. **125**(7), 074906 (2006).
[23]J. M. Kim and P. S. Doyle, Lab Chip **7**(2), 213–225 (2007).
[24]M. Z. Bazant and T. M. Squires, Phys. Rev. Lett. **92**(6), 066101 (2004).
[25]M. Z. Bazant, K. Thornton, and A. Ajdari, Phys. Rev. E **70**(2), 021506 (2004).
[26]J. Ou, J. Cho, D. W. Olson, and K. D. Dorfman, Phys. Rev. E **79**(6), 061904 (2009).
[27]G. C. Randall and P. S. Doyle, Proc. Natl. Acad. Sci. U. S. A. **102**(31), 10813–10818 (2005).
[28]Y. J. Juang, X. Hu, S. N. Wang, L. J. Lee, C. M. Lu, and J. J. Guan, Appl. Phys. Lett. **87**(24), 244105 (2005).
[29]J. Tang, N. Du, and P. S. Doyle, Proc. Natl. Acad. Sci. U. S. A. **108**(39), 16153–16158 (2011).
[30]R. G. Larson, H. Hu, D. E. Smith, and S. Chu, J. Rheol. **43**(2), 267–304 (1999).
[31]L. Fang, C. C. Hsieh, and R. G. Larson, Macromolecules **40**(23), 8490–8499 (2007).
[32]L. Fang and R. G. Larson, Macromolecules **40**(24), 8784–8787 (2007).
[33]K. Jo, Y. L. Chen, J. J. de Pablo, and D. C. Schwartz, Lab Chip **9**(16), 2348–2355 (2009).
[34]Y. L. Chen, M. D. Graham, J. J. de Pablo, K. Jo, and D. C. Schwartz, Macromolecules **38**(15), 6680–6687 (2005).
[35]R. M. Jendrejack, E. T. Dimalanta, D. C. Schwartz, M. D. Graham, and J. J. de Pablo, Phys. Rev. Lett. **91**(3), 038102 (2003).
[36]R. M. Jendrejack, D. C. Schwartz, J. J. de Pablo, and M. D. Graham, J. Chem. Phys. **120**(5), 2513–2529 (2004).
[37]H. B. Ma and M. D. Graham, Phys. Fluids **17**(8), 083103 (2005).
[38]Y. L. Chen, M. D. Graham, J. J. de Pablo, G. C. Randall, M. Gupta, and P. S. Doyle, Phys. Rev. E **70**(6), 060901(R) (2004).
[39]A. Balducci, P. Mao, J. Y. Han, and P. S. Doyle, Macromolecules **39**(18), 6273–6281 (2006).
[40]C. C. Hsieh, A. Balducci, and P. S. Doyle, Macromolecules **40**(14), 5196–5205 (2007).
[41]R. G. Larson, Rheol. Acta **31**(6), 497–520 (1992).
[42]K. A. Dill and B. H. Zimm, Nucleic Acids Res. **7**(3), 735–749 (1979).